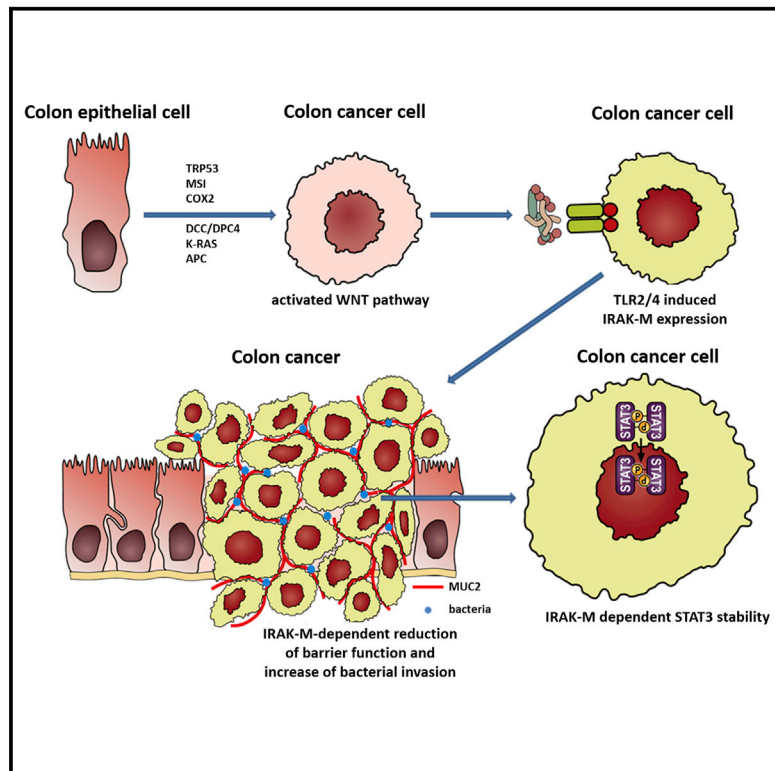


Cancer Cell

IRAK-M Expression in Tumor Cells Supports Colorectal Cancer Progression through Reduction of Antimicrobial Defense and Stabilization of STAT3

Graphical Abstract



Authors

Rebecca Kesselring,
Joachim Glaesner,
Andreas Hiergeist, ...,
Hans-Juergen Schlitt,
Edward K. Geissler,
Stefan Fichtner-Feigl

Correspondence

stefan.fichtner@ukr.de

In Brief

Kesselring et al. show that combined TLR and Wnt activation leads to IRAK-M expression in colorectal cancer cells, which is also associated with poor patient prognosis. Tumor cell-intrinsic IRAK-M regulates antimicrobial response and STAT3 stability, both promoting tumor progression.

Highlights

- IRAK-M deficiency results in enhanced inflammation but diminished tumor growth
- IRAK-M is induced in colon tumor cells due to combined Wnt and TLR activation
- IRAK-M in tumor cells stabilizes STAT3 and enhances tumor barrier
- IRAK-M expressed in tumor cells of CRC patients is associated with poor prognosis



IRAK-M Expression in Tumor Cells Supports Colorectal Cancer Progression through Reduction of Antimicrobial Defense and Stabilization of STAT3

Rebecca Kesselring,¹ Joachim Glaesner,² Andreas Hiergeist,² Elisabeth Naschberger,³ Helmut Neumann,⁴ Stefan M. Brunner,¹ Anja K. Wege,⁵ Caroline Seebauer,¹ Gudrun Köhl,¹ Susanne Merkl,³ Roland S. Croner,³ Christina Hackl,¹ Michael Stürzl,³ Markus F. Neurath,⁴ André Gessner,² Hans-Juergen Schlitt,¹ Edward K. Geissler,¹ and Stefan Fichtner-Feigl^{1,6,*}

¹Department of Surgery

²Institute of Microbiology and Hygiene

University Medical Center Regensburg, Franz-Josef-Strauß-Allee 11, 93053 Regensburg, Germany

³Department of Surgery, University Medical Center Erlangen, Schwabachanlage 12, 91054 Erlangen, Germany

⁴Department of Internal Medicine, University Medical Center Erlangen, Ulmenweg 18, 91054 Erlangen, Germany

⁵Clinic of Gynecology and Obstetrics, Caritas Hospital St. Josef, University of Regensburg, 93053 Regensburg, Germany

⁶Regensburg Center for Interventional Immunology, University Medical Center Regensburg, Franz-Josef-Strauß-Allee 11, 93053 Regensburg, Germany

*Correspondence: stefan.fichtner@ukr.de

<http://dx.doi.org/10.1016/j.ccell.2016.03.014>

SUMMARY

Colorectal cancer (CRC) is associated with loss of epithelial barrier integrity, which facilitates the interaction of the immunological microenvironment with the luminal microbiome, eliciting tumor-supportive inflammation. An important regulator of intestinal inflammatory responses is IRAK-M, a negative regulator of TLR signaling. Here we investigate the compartment-specific impact of IRAK-M on colorectal carcinogenesis using a mouse model. We demonstrate that IRAK-M is expressed in tumor cells due to combined TLR and Wnt activation. Tumor cell-intrinsic IRAK-M is responsible for regulation of microbial colonization of tumors and STAT3 protein stability in tumor cells, leading to tumor cell proliferation. IRAK-M expression in human CRCs is associated with poor prognosis. These results suggest that IRAK-M may be a potential therapeutic target for CRC treatment.

INTRODUCTION

Colorectal carcinoma (CRC) represents the third most prevalent malignancy and is one of the leading causes of cancer-related deaths worldwide. The etiology of CRC is known to be multifactorial and is associated with predisposing mutations, diet, lifestyle, chronic inflammations, and gut microbiota (Balkwill and Mantovani, 2001; Gallimore and Godkin, 2013; Goel et al., 2011). Inflammation is a critical player in the development of both colitis-associated cancer (CAC) and sporadic CRC, and influences all stages of CRC pathogenesis including initiation, progression, and metastasis. Ongoing research has confirmed

that the gut microbiome is an important driver of inflammation and is linked to the pathogenesis of CRC (Arthur and Jobin, 2013; Jobin, 2013). The colon harbors more than 36,000 bacterial entities, amounting to more than 100 trillion aerobic and anaerobic bacteria (Ohtani, 2014). In steady state the intestine is in crosstalk with its microbiome, thereby maintaining intestinal homeostasis. In this regard, *Streptococcus bovis/galolyticus*, enterotoxigenic *Bacteroides fragilis*, and *Escherichia coli* NC101 have been implicated as risk factors for CRC (Arthur et al., 2012; Grivennikov, 2013). However, the precise mechanisms are far from being understood. Disruption of the intestinal homeostasis due to loss of epithelial barrier integrity enables activation

Significance

Despite advances in the diagnosis, surgery, and therapy of colorectal cancer (CRC), only minor improvements have been achieved in the clinical outcome of CRC patients. Here we show that IRAK-M, an inhibitor of TLR signaling, is expressed in tumor cells and is associated with enhanced tumor cell proliferation. This could be explained through our findings that IRAK-M supports barrier breach at tumor sites through inhibition of antimicrobially acting proteins and is responsible for STAT3 stability in tumors. IRAK-M expression in human CRCs is associated with poor prognosis. These results suggest that IRAK-M may be a potential therapeutic target for the treatment of CRC.

of immune responses through triggering of microbial sensors, namely the pathogen recognition receptors (PRRs) (Pandey et al., 2014). The sensing of microbial pathogen-associated molecular patterns by PRRs activates signaling pathways involved in inflammatory responses (Fukata and Arditi, 2013; McDermott and Huffnagle, 2014). These pathways lead to the secretion of proinflammatory cytokines such as interleukin-1 β (IL-1 β), IL-6, IL-11, and tumor necrosis factor (TNF) triggering the activation of nuclear factor κ B (NF- κ B) and STAT3 in intestinal epithelial cells (IECs). Both NF- κ B and STAT3 are activated in CRCs, leading to the induction of genes for cell proliferation and survival, and are well described to be major players in the pathogenesis of CRCs (Ben-Neriah and Karin, 2011; Bollrath and Greten, 2009; Bollrath et al., 2009). There are extensive studies describing the crucial role of PRRs in CRC pathogenesis, especially Toll-like receptors (TLRs) and nucleotide oligomerization domain (NOD)-like receptors and their downstream molecules MyD88 and RIP2, respectively (Couturier-Maillard et al., 2013; Fukata and Abreu, 2009; Fukata et al., 2011; Rakoff-Nahoum and Medzhitov, 2007; Salcedo et al., 2010). Therefore, it is essential that sensing of microbes through PRRs and their downstream signaling pathways are tightly regulated. Negative regulators of PRR signaling include A20, IRAK-M, SIGIRR, Tollip, SOCS1, and PPAR γ . It is already described that A20 suppresses colorectal cancerogenesis through restriction of Wnt signaling and that SIGIRR deficiency enhances tumor promotion and progression through hyperactivation of the NF- κ B and STAT3 signaling pathways, but less is known about the other inhibitory molecules for TLR signaling (Shao et al., 2013; Xiao et al., 2007). IRAK-M is a member of the IL-1 receptor-associated kinases (IRAK) family of adaptor molecules (Kobayashi et al., 2002). In contrast to other IRAK family members, IRAK-M lacks kinase activity. IRAK-M blocks the formation of IRAK-1/TRAF6 complexes, preventing dissociation of IRAK-1/IRAK-4 from the TLR receptor and thereby inhibiting downstream signaling and activation of NF- κ B (Shibolet and Podolsky, 2007). In the gut, IRAK-M is described as an important factor for the establishment of epithelial barrier integrity. Hence, it was shown that the absence of IRAK-M exacerbates colitis in IL-10-deficient mice as well as in acute dextran sodium sulfate (DSS) colitis by deregulation of proinflammatory cytokines and T helper 1 (Th1)- and Th17-inducing cytokines (Berglund et al., 2010; Biswas et al., 2011). However, less is known about the impact of IRAK-M on tumor pathogenesis. Here, we analyzed the role of IRAK-M in the development of CRCs.

RESULTS

IRAK-M Protects against Colitis but Enhances Tumor Growth

It is already described that IRAK-M protects against colitis in IL-10 $^{-/-}$ mice and in acute DSS colitis (Berglund et al., 2010; Biswas et al., 2011). Therefore, it is reasonable to analyze the impact of IRAK-M on the progression of chronic colitis and CRC. In the azoxymethane (AOM)/DSS model of CAC we observed severe signs of intestinal inflammation in IRAK-M $^{-/-}$ mice and significant weight loss compared with wild-type (WT) mice (Figures 1A and S1A–S1C). Histologically, IRAK-M $^{-/-}$ mice present a significant extent of inflammation throughout the mucosa,

alterations of epithelial structure, loss of crypts, and enhanced lymphocytic infiltration compared with WT mice (Figure 1B). IRAK-M $^{-/-}$ mice have a significantly elevated histopathological score (Figure 1C). The enhanced inflammation is accompanied by dense infiltration of CD45 $^{+}$ lymphocytes in the lamina propria (Figures 1D and S1D). Despite an increase in inflammation, we observed a decreased tumor load in IRAK-M-deficient mice compared with WT mice despite unchanged Wnt activation in tumor cells, as shown by nuclear β -catenin staining and active β -catenin levels (Figures 1E and 1F). Whereas about 92% of the WT mice developed colon tumors, only 57% of IRAK-M $^{-/-}$ mice developed macroscopic tumors or polyps in the distal colon. In particular, IRAK-M $^{-/-}$ mice showed both decreased tumor numbers and reduced tumor size (Figures 1G–1J). The average tumor number per mouse in WT mice (19 ± 1.7) was about three times higher than that in IRAK-M $^{-/-}$ mice (6 ± 1.5) (Figure 1H). Regarding tumor size, about 61% of the tumors of WT mice developed into large tumors (>2 mm diameter) whereas only 5% of IRAK-M $^{-/-}$ tumors developed into large tumors with histological characteristics of adenocarcinoma (Figure 1J). In contrast, 64% of the IRAK-M $^{-/-}$ tumors are small tumors (<1 mm diameter) and only 12% of the WT tumors are small (Figure 1J). These results indicate that IRAK-M deficiency not only diminishes tumor promotion but also decreases tumor progression. This observed phenomenon seems to be contradictory to previous studies of CAC in which enhanced inflammation was associated with accelerated tumor growth (Balkwill and Mantovani, 2001; Clevers, 2004). To understand this observation, we analyzed the immunological tumor milieu of IRAK-M-deficient mice in depth. Lamina propria mononuclear cells (LPMCs) of WT and IRAK-M $^{-/-}$ mice show increased absolute amounts of CD45 $^{+}$ lymphocytes (Figures 1D and S1D). Flow cytometric analysis revealed that in the late phase the tumor-associated immune milieu is not altered in IRAK-M $^{-/-}$ mice in respect of percentage of special subpopulations of LPMC-infiltrating lymphocytes. There are similar relative amounts of T cells, regulatory T (Treg) cells, Th1, and Th17 cells in the lamina propria of WT and IRAK-M $^{-/-}$ mice (Figure S1E), and the percentages of dendritic cells, monocytes, and macrophages are also similar (Figure S1E). Antigen-presenting cells produce the same amount of the proinflammatory cytokines (Figure S1E). The analysis of the chemokine milieu of the inflamed colon of IRAK-M $^{-/-}$ and WT mice, however, revealed a strong upregulation of various chemokines such as CCL1, 3, 4, 5, 7 and 22, and the chemokines CXCL1, 2, 3 and 5 in IRAK-M $^{-/-}$ mice (Figure S1F). The TLR signaling pathway leads to activation of the transcription factor NF- κ B. We analyzed the NF- κ B pathway in IRAK-M $^{-/-}$ and WT mice treated with AOM/DSS. We found hardly any differences both in the canonical and in the non-canonical NF- κ B pathways (Figure S1G). To better assess the course of inflammation and understand the underlying inflammatory responses, we performed acute DSS colitis and time course analysis of chronic DSS colitis as well as AOM/DSS colitis (Figures S1H–S1P). Here it becomes clear that IRAK-M is mostly involved in the regulation of early and acute phases of inflammation and has a limited regulatory role in late and chronic phases. In acute DSS colitis, there is complete damage to epithelial structure in acute DSS colitis (Figures S1H–S1J) with persistently enhanced CD45 $^{+}$ cell infiltrates in

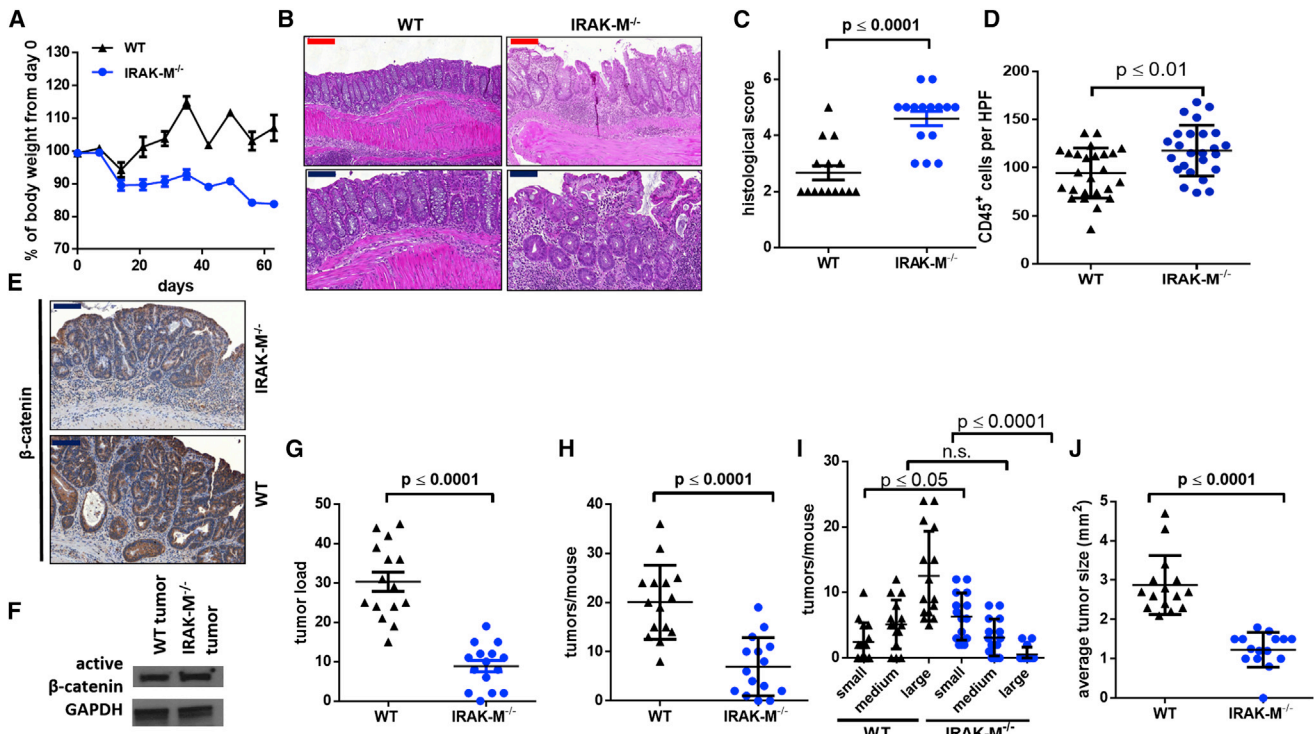


Figure 1. IRAK-M Protects against Colitis but Enhances Tumor Growth

(A) Body weight curve of WT and IRAK-M^{-/-} mice during the course of AOM/DSS colitis. Data are mean ± SD; n = 15.

(B) H&E-stained sections of colons from WT and IRAK-M^{-/-} mice after AOM/DSS colitis (day 63), showing representative inflammation.

(C) Histopathological score of WT and IRAK-M^{-/-} mice analyzed from distal colonic tissue sections at the end of AOM/DSS colitis (day 63). Each dot represents the histological score of one individual mouse. The horizontal bar represents the mean ± SD (n = 15); p ≤ 0.0001 by t test.

(D) Analysis of CD45⁺ infiltrating immune cells in colons of IRAK-M^{-/-} and WT mice after AOM/DSS colitis (day 63). Each dot represents the number of CD45⁺ cells in one high-power field imaged from the colon of the specified AOM/DSS-treated mice. The horizontal bar represents the mean ± SD (n = 25); p ≤ 0.01 by t test.

(E) Immunohistochemical analysis of β-catenin in colorectal tumors of WT and IRAK-M^{-/-} mice after treatment with AOM/DSS (day 63).

(F) Immunoblot analysis of active β-catenin from whole-cell protein lysates from IECs and tumors of IRAK-M^{-/-} mice compared with WT mice after AOM/DSS colitis (day 63). GAPDH represents the loading control.

(G) Tumor load of WT and IRAK-M^{-/-} mice after AOM/DSS colitis (day 63). Data points represent the tumor load of one individual mouse. The horizontal bar represents the mean ± SD (n = 15); p ≤ 0.0001 by t test.

(H) Tumor count per mice of WT and IRAK-M^{-/-} mice after treatment with AOM/DSS. Data represent the number of tumors detected in one individual mouse. The horizontal bar represents the mean ± SD (n = 15); p ≤ 0.0001 by t test.

(I) Count of small, medium, and large tumors per mouse of WT and IRAK-M^{-/-} mice after AOM/DSS colitis. Data points represent the tumor load of one individual mouse. The horizontal bar represents the mean ± SD (n = 15); p ≤ 0.05 for small tumors, not significant (n.s.) for medium tumors, and p ≤ 0.0001 for large tumors by t test.

(J) Average of tumor sizes in WT and IRAK-M^{-/-} mice after treatment with AOM/DSS. Data represent the average tumor size in one individual mouse. The horizontal bar represents the mean ± SD (n = 15); p ≤ 0.0001 by t test.

Blue scale bar, 100 μm; red scale bar, 200 μm. See also Figure S1.

IRAK-M^{-/-} mice (Figures S1K–S1L). In late phases the inflammation in IRAK-M^{-/-} mice remains constant, whereas the inflammation in WT mice still increases accompanied by enhanced CD45⁺ lymphocyte infiltration, and the infiltration of lymphocytes in IRAK-M^{-/-} colon remains constant after the acute phase of colitis (Figures S1M–S1P). In studies of immune cell activation, we found major differences in the acute phase of colitis but only minor differences in the chronic phase (Figure S1Q). In summary, we have shown that despite exacerbated colitis in IRAK-M^{-/-} mice, there have to be protective mechanisms that inhibit the inflammation-induced colorectal carcinogenesis that is normally observed in an inflamed tumor microenvironment.

Epithelial IRAK-M Is Necessary for Sustained Colorectal Cancerogenesis, whereas Hematopoietic IRAK-M Slows Down Inflammation-Associated Cancer Progression

As reduced tumorigenesis in IRAK-M-deficient mice in a milieu of severe inflammation at first sight seems to be contradictory to the hypothesis that inflammation fuels tumorigenesis, we investigated whether the observed decelerated tumor progression is solely an immune cell-associated effect. Therefore, we generated bone marrow (BM) chimera of IRAK-M^{-/-} mice. We included four different groups; IRAK-M^{-/-} mice that received WT BM (WT BM > IRAK-M^{-/-}), WT mice that received IRAK-M^{-/-} BM (IRAK-M^{-/-} BM > WT), and two control groups of IRAK-M^{-/-} mice that received IRAK-M^{-/-} BM (IRAK^{-/-}

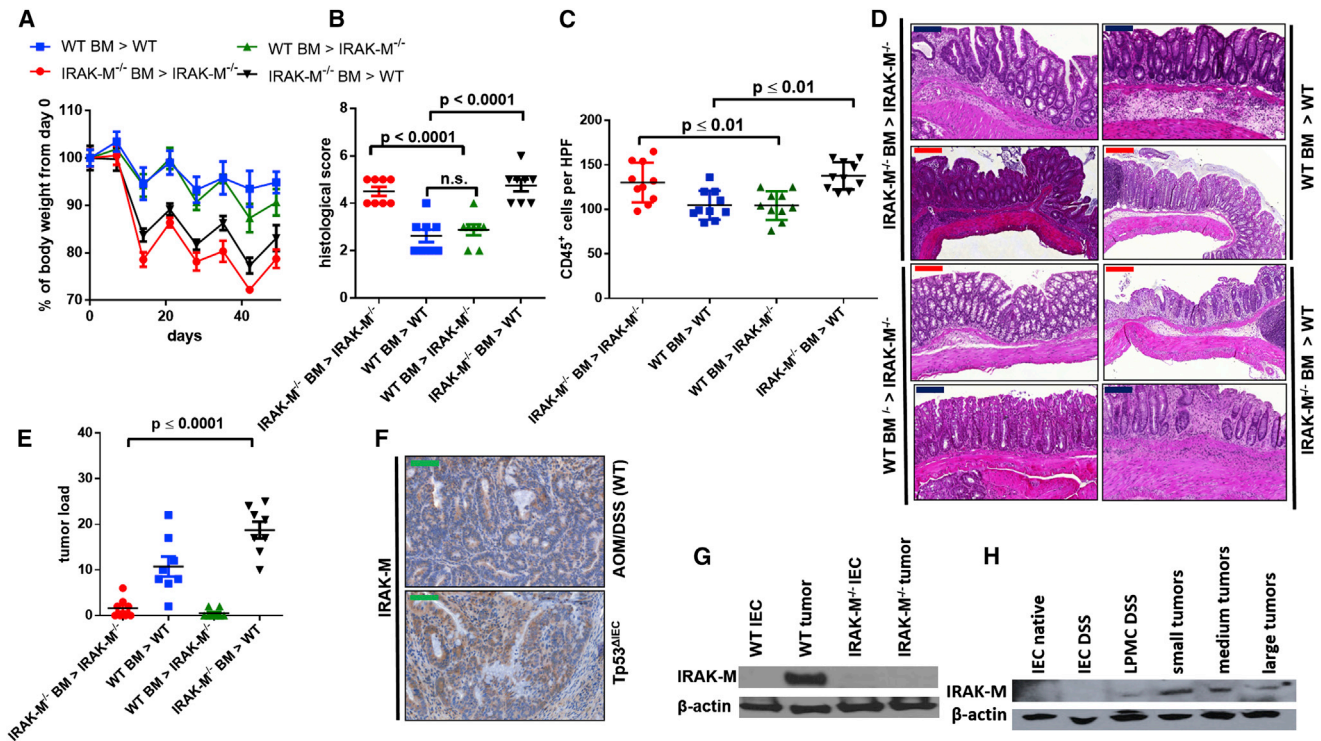


Figure 2. Epithelial IRAK-M Is Necessary for Sustained Colorectal Cancerogenesis whereas Hematopoietic IRAK-M Slows Down Inflammation-Associated Cancer Progression

(A) Body weight curve of BM chimera of WT BM > WT, IRAK-M^{-/-} BM > IRAK-M^{-/-}, IRAK-M^{-/-} BM > WT, and WT BM > IRAK-M^{-/-} mice during the course of AOM/DSS colitis. Data are mean ± SD; n = 8.

(B) Histopathological score of BM chimera of WT BM > WT, IRAK-M^{-/-} BM > IRAK-M^{-/-}, IRAK-M^{-/-} BM > WT, and WT BM > IRAK-M^{-/-} mice after AOM/DSS colitis (day 63). Each dot represents the histological score of one individual mice. The horizontal bar represents the mean ± SD (n = 8); p ≤ 0.0001 by t test.

(C) Analysis of CD45⁺ infiltrating immune cells in colons from BM chimera of WT BM > WT, IRAK-M^{-/-} BM > IRAK-M^{-/-}, IRAK-M^{-/-} BM > WT, and WT BM > IRAK-M^{-/-} mice after AOM/DSS colitis (day 63). Each dot represents the number of CD45⁺ cells in one high-power field imaged from the colon of the specified AOM/DSS-treated mice. The horizontal bar represents the mean ± SD (n = 25); p ≤ 0.01 by t test.

(D) H&E-stained sections of colons from BM chimera of WT BM > WT, IRAK-M^{-/-} BM > IRAK-M^{-/-}, IRAK-M^{-/-} BM > WT, and WT BM > IRAK-M^{-/-} mice after AOM/DSS colitis (day 63), showing representative inflammation.

(E) Tumor load of BM chimera of WT BM > WT, IRAK-M^{-/-} BM > IRAK-M^{-/-}, IRAK-M^{-/-} BM > WT, and WT BM > IRAK-M^{-/-} mice after AOM/DSS colitis (day 63). Data points represent the tumor load of one individual mouse. The horizontal bar represents the mean ± SD (n = 8); p ≤ 0.0001 by t test.

(F) Immunohistochemical analysis of IRAK-M in colorectal tumors of Tp53^{ΔIEC} mice 16 weeks after the first of six weekly AOM injections (lower panel) and WT mice treated with AOM/DSS (day 63) (upper panel).

(G) Immunoblot analysis for IRAK-M in lysates from IECs and tumors of WT and IRAK-M^{-/-} mice after AOM/DSS treatment (day 63). β-Actin represents the loading control.

(H) Immunoblot analysis for IRAK-M in lysates from native and AOM/DSS-treated IECs, AOM/DSS-treated LPMCs, and different sizes of tumors (small, medium, large) of WT mice after AOM/DSS treatment (day 63). β-Actin represents the loading control.

Green scale bar, 50 μm; blue scale bar, 100 μm; red scale bar, 200 μm. See also Figure S2.

BM > IRAK-M^{-/-}) and WT mice that received WT BM (WT BM > WT). During chronic colitis, mice that received IRAK-M^{-/-} BM showed more severe weight loss and increased histology score than mice with WT BM (Figures 2A, 2B, and S2A–S2C). Further, IRAK-M deficiency in the irradiation-insensitive compartment hardly had any impact on the extent of inflammation, as depicted by the weight curves and histology score (Figures 2A and 2B). H&E staining also showed severe inflammation in mice with IRAK-M-deficient BM with elevated levels of CD45⁺ lymphocytic infiltrations (Figures 2C and 2D) and a high percentage of mucosal damage represented by a high histopathological score (Figure 2B). Regarding tumorigenesis, mice with an IRAK-M-deficient, irradiation-insensitive compartment showed reduced

tumor load compared with the WT control group (Figure 2E), whereas a deficiency of IRAK-M in the BM led to an enhanced tumor progression (Figure 2E). Mice deficient for IRAK-M in the irradiation-insensitive compartment showed smaller tumor size and diminished tumor incidence compared with mice with a WT epithelial compartment (Figures S2D–S2F). β-Catenin staining revealed a shift of catenin expression from the membrane toward cytoplasmic and nuclear localization in tumor regions in all four groups, indicating no obvious difference in tumor formation between WT and IRAK-M^{-/-} mice (Figure S2G). As these results suggest that IRAK-M is able to exert an epithelial cell-intrinsic effect in the irradiation-insensitive compartment, we analyzed IRAK-M expression in different CRC models (AOM/DSS and

Tp53^{ΔIEC} models) and in human CRC cell lines. We demonstrated that IRAK-M is expressed in tumor cells of CRC in both mouse models and in a diverse set of well-established CRC cell lines (Figures 2F–2G, S2H, and S2I). Untransformed/non-tumorous IECs did not express IRAK-M in the AOM/DSS and Tp53^{ΔIEC} models (Figures 2G and S2H). Deeper analysis of IRAK-M expression in the gastrointestinal tract revealed that neither native IEC- nor DSS-treated IECs show IRAK-M expression (Figure 2H) whereas LPMCs, most likely macrophages, show positive IRAK-M staining (Figure 2H). Comparison of different tumor sizes revealed that IRAK-M is expressed to a rather similar degree irrespective of tumor size (Figure 2H). To confirm that IRAK-M is expressed specifically in tumor cells of CRCs, we performed co-staining analysis of colonic tissue of the different cell types present in the colon (fibroblasts, lymphocytes, tumor cells, and endothelial cells) in WT mice (Figures S2J–S2M). IRAK-M is expressed neither in endothelial cells nor fibroblasts but is expressed in tumor cells and partially infiltrating lymphocytes (Figures S2J–S2M).

IRAK-M Is Induced in Epithelial Cells through Combined TLR2/4 and Wnt Activation and Is per se Associated with Altered Fecal Gut Microbiota Composition and Bacterial Diversity

The specific expression of IRAK-M in tumor cells but not in untransformed/non-tumorous IECs raises the question as to how IRAK-M is induced in tumor cells. As IRAK-M is known to be involved in TLR signaling, we hypothesized that TLR activation is involved in IRAK-M induction. Additionally, we hypothesized that the activation of the Wnt pathway might be involved in the induction of IRAK-M expression, as its aberrant activation pattern is a prominent difference between tumor cells and untransformed IECs. To verify this hypothesis, we stimulated the murine and human IEC cell lines mIntepi and HCoEpiC with different TLR ligands (TLRs 1–9) and with the Wnt agonist I, and analyzed for IRAK-M expression by western blotting. Indeed, we found an upregulation of IRAK-M protein expression under simultaneous TLR4 and Wnt activation and under TLR2 and Wnt activation (Figures 3A, S3A, and S3B). Additionally, we demonstrated that intrarectal administration of Wnt with TLR2 or TLR4 agonist also induced IRAK-M expression in IECs in vivo (Figure 3A). In mice with loss of TLR signaling (MyD88^{-/-}) we saw a slight decrease in IRAK-M induction (Figure S3C).

We then analyzed whether this close interaction was associated with changes in the composition of the intestinal microbiome of IRAK-M^{-/-} mice compared with WT mice. In feces of IRAK-M^{-/-} mice, the total bacterial content was approximately 8-fold lower than in WT mice as reflected by the amount of 16S-rDNA gene copies (Figure 3B). In addition, estimating the species richness of the microbiome in feces samples we detected a more diverse composition of bacteria in WT mice compared with IRAK-M^{-/-} mice (Figure 3B). When analyzing the data obtained from the deep 16S-rRNA sequencing on a taxonomical level, some striking differences were identified. Thus, some bacterial taxa (*Roseburia*, *Blautia*, *Parasutterella*) were found to be markedly less abundant or nearly absent in IRAK-M^{-/-} feces, whereas others were more abundant (*Turicibacter* and further undefined members of the Erysipelotrichaceae family) (Figure 3C). Similar differences regarding these

bacterial taxa could also be observed in a replicate experiment which additionally included colonic and tumor tissue of the respective mice (Figures S3E–S3H). In these colon and tumor tissues differences in the species richness between the two groups similar to those in luminal microbiota were observed (Figure S3H). Assessing the diversity of the fecal microbiota between IRAK-M^{-/-} and WT mice by a principal coordinates analysis, we found that all samples derived from IRAK-M^{-/-} mice clustered apart from those of WT controls (Figure 3D), although we revealed less overall microbial content in IRAK-M^{-/-} mice with less diversity and fewer changes in taxa distribution.

To analyze whether the reduced bacterial content as shown in Figures 3E and S3E–S3H in IRAK-M^{-/-} mice is a consequence of a more intact epithelial barrier or of enhanced antibacterial responses, we analyzed antibacterial responses and intestinal permeability separately from non-tumorous epithelium and tumor sites, comparing WT and IRAK-M^{-/-} mice. This is of particular importance, as the local barrier function at tumor sites fuels tumorigenesis, as shown by Grivennikov et al. (2012) and Schwitalla et al. (2013). Regarding non-tumorous epithelium, we demonstrated that intestinal permeability is increased in IRAK-M^{-/-} mice as indicated by fluorescein isothiocyanate dextran measurements (Figure S3J). Furthermore, the number of translocated bacteria was increased in mesenteric lymph nodes of IRAK-M^{-/-} mice (Figure S3N). We evaluated the mucus layer thickness on the colonic epithelium and observed a decreased thickness of this layer in IRAK-M^{-/-} mice (Figures S3L and S3M). Periodic acid-Schiff staining revealed no differences in the number of goblet cells in the colon of WT and IRAK-M^{-/-} mice (Figure S3D). Finally, evaluation of tight junction protein expression showed reduced ZO-1 expression in IRAK-M^{-/-} IECs but no difference in the tight junction architecture in tumors (Figures S3I and S3K). In contrast to inflamed colonic epithelium, at tumor sites we found highly increased Mucin2 deposition and enhanced expression of the antibacterial peptides Galectin 8 and Cathelicidin in tumors from IRAK-M^{-/-} mice (Figure 3E and 3F). In conclusion, we found a barrier breach in the inflamed intestine of IRAK-M^{-/-} mice on various levels. At tumor sites of IRAK-M^{-/-} mice we found highly increased antibacterial response and barrier function, suggesting that luminal bacteria cannot translocate into IRAK-M^{-/-} tumors.

The Exaggerated Colitis of IRAK-M^{-/-} Mice Is Transmissible through the IRAK-M^{-/-} Microbiota, whereas Tumorigenesis in IRAK-M^{-/-} Mice Is Independent of the Present Microbiota

The verified differences in the microbiota of IRAK-M^{-/-} mice in combination with alterations in antibacterial responses in tumors of IRAK-M^{-/-} mice led us to ask whether bacterial dysbiosis is the basis for the exacerbated colitis and reduced tumorigenesis in IRAK-M^{-/-} mice or is merely a consequence of the underlying disorder. Therefore, we performed co-housing experiments with IRAK-M-deficient and WT mice to study the alterations in inflammation and tumor growth in the AOM/DSS model depending on the quantity and quality of the different microbiota. We compared four different groups of WT mice that were co-housed with IRAK-M^{-/-} mice (IRAK-M^{-/-} MB > WT), IRAK-M^{-/-} mice that were co-housed with WT mice (WT MB > IRAK-M^{-/-}), and single-housed IRAK-M^{-/-} mice (IRAK-M^{-/-} MB > IRAK-M^{-/-})

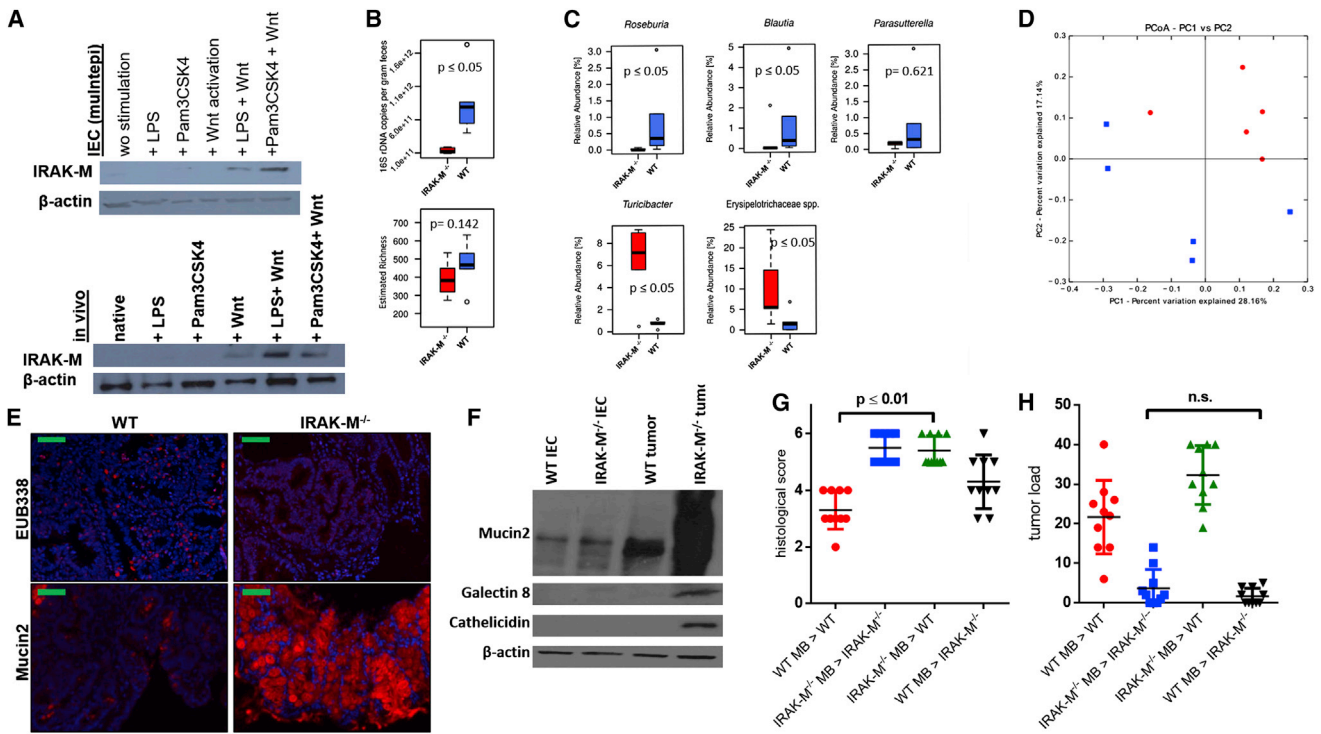


Figure 3. IRAK-M Is Induced in Epithelial Cells through Combined TLR2/4 and Wnt Activation and Is per se Associated with Altered Fecal Gut Microbiota Composition and Bacterial Diversity

(A) Upper panel: immunoblot analysis for IRAK-M in lysates from the IEC lineage multitepi stimulated with different TLR ligands (LPS, Pam3CSK4) \pm Wnt activation. β -Actin represents the loading control. Lower panel: immunoblot analysis for IRAK-M in lysates from IECs isolated from mice intrarectally treated with different TLR ligands (LPS, Pam3CSK4) \pm Wnt activation. β -Actin represents the loading control.

(B) Total eubacterial 16S-rDNA copies per gram of feces as measured by qPCR and Chao1 richness estimation in IRAK-M^{-/-} (n = 5) and WT (n = 5) mice. The individual points that are plotted as open circles beyond the whiskers represent values deviating from the box by more than 1.2-fold interquartile range. Differences were tested for significance using the Kruskal-Wallis rank-sum test.

(C) Differential abundance of selected bacterial taxa in stool samples of IRAK-M^{-/-} (n = 5) and WT (n = 5) mice. The individual points that are plotted as open circles beyond the whiskers represent values deviating from the box by more than 1.2-fold interquartile range. Differences were tested for significance using the Kruskal-Wallis rank-sum test ($p \leq 0.05$).

(D) Analysis of beta diversity between stool samples of IRAK-M^{-/-} (red circles) and WT (blue squares) tumors of AOM/DSS-treated mice (day 63) by principal coordinates analysis (PCoA) of unweighted UniFrac distances.

(E) Fluorescence in situ hybridization analysis using a Cy3-labeled universal eubacteria probe (EUB 338) of WT and IRAK-M^{-/-} tumors (upper panel) and immunofluorescence analysis of Mucin2 (lower panel) in tumors of WT and IRAK-M^{-/-} mice at day 63 of AOM/DSS colitis. Scale bar, 50 μ m.

(F) Immunoblot analysis for different antimicrobial acting proteins (Mucin2, Cathelicidin, and Galectin 8) in lysates from IECs and tumors of WT and IRAK-M^{-/-} mice after AOM/DSS treatment (day 63). β -Actin represents the loading control.

(G) Histopathological score of single-housed WT and IRAK-M^{-/-} mice (WT MB > WT, IRAK-M^{-/-} MB > IRAK-M^{-/-}) and co-housed WT and IRAK-M^{-/-} (WT MB > IRAK-M^{-/-}, IRAK-M^{-/-} MB > WT) mice. Each dot represents the histological score of one individual mouse analyzed after AOM/DSS colitis (day 63). The horizontal bar represents the mean \pm SEM (n = 10); $p \leq 0.01$ by t test.

(H) Tumor load of single-housed WT and IRAK-M^{-/-} mice (WT MB > WT, IRAK-M^{-/-} MB > IRAK-M^{-/-}) and co-housed WT and IRAK-M^{-/-} (WT MB > IRAK-M^{-/-}, IRAK-M^{-/-} MB > WT) mice after AOM/DSS colitis (day 63). Data points represent the tumor load of one individual mouse. The horizontal bar represents the mean \pm SEM (n = 10); $p \leq 0.0001$ by t test.

See also Figure S3.

and single-housed WT mice (WT MB > WT). Mice that were confronted with microbiota from IRAK-M^{-/-} mice showed more intestinal inflammation than mice only confronted with WT microbiota, as unveiled by a greater loss of body weight and a higher histological score (Figures 3G and S3O–S3S). Despite these differences in induction of an inflammatory response, co-housing of WT and IRAK-M^{-/-} mice has no influence on tumor growth in IRAK-M^{-/-} mice, whereas tumorigenesis in WT mice confronted with IRAK-M^{-/-} microbiota is enhanced through the increased inflammation (Figures 3H and S3T–S3V). β -Catenin staining showed no altered nuclear expression patterns between

the four groups (Figure S3W). Therefore, we conclude that the colitis of IRAK-M^{-/-} mice is transmissible and the microbiota of IRAK-M^{-/-} mice has characteristics of a protumoral-acting microbiome, but the reduction in tumorigenesis in IRAK-M^{-/-} mice is microbiota independent.

Tumor Cell-Associated IRAK-M Facilitates Tumor Growth through Stabilization of STAT3

It is questionable whether the elevated antimicrobial defense mechanisms in IRAK-M-deficient mice are the main alterations that sufficiently explain the picture of rigorously reduced tumor

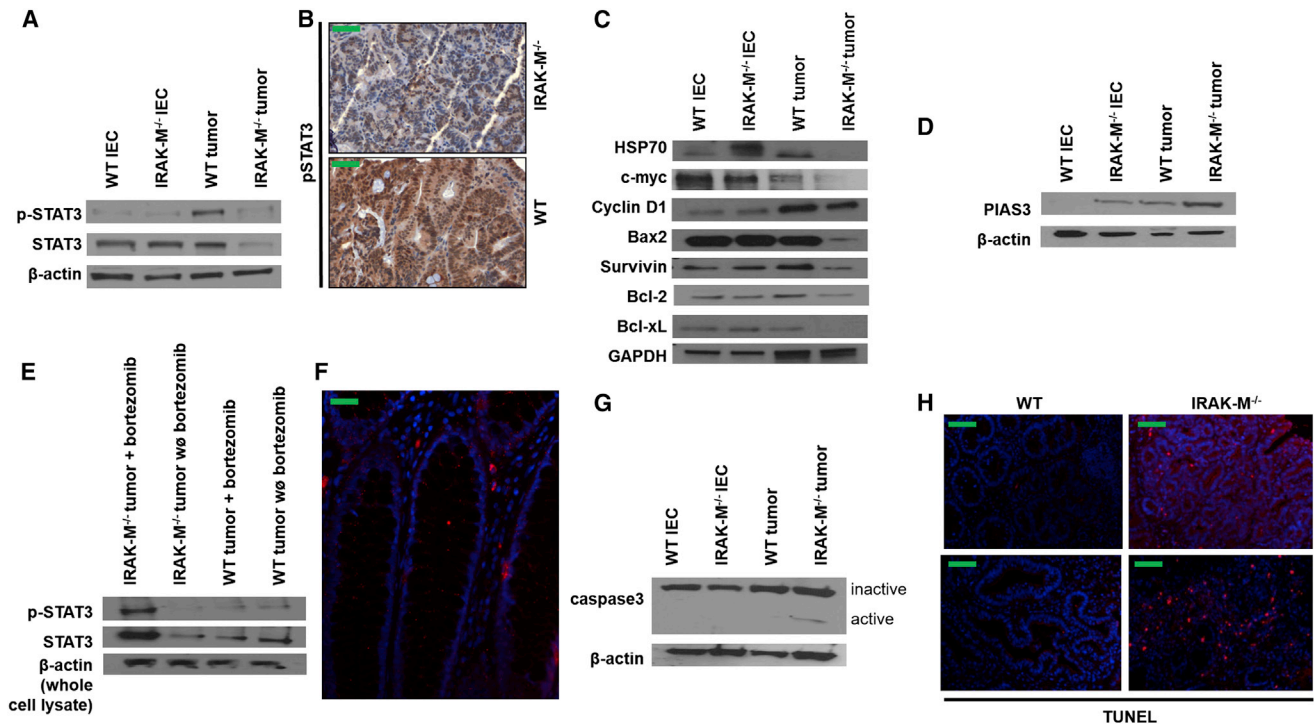


Figure 4. Tumor Cell-Associated IRAK-M Facilitates Tumor Growth through Stabilization of STAT3

(A) Immunoblot analysis for phospho-STAT3 and STAT3 in lysates from IECs and tumors of WT and IRAK-M^{-/-} mice after AOM/DSS treatment (day 63). β-Actin represents the loading control.

(B) Immunohistochemical analysis for phospho-STAT3 in tumors of WT and IRAK-M^{-/-} mice after AOM/DSS colitis (day 63).

(C) Immunoblot analysis for different downstream targets of STAT3 in lysates from IECs and tumors of WT and IRAK-M^{-/-} mice after AOM/DSS treatment (day 63). Downstream targets analyzed are Hsp 70, Cyclin D1, Bax2, Survivin, Bcl2, and Bcl-xL. GAPDH represents the loading control.

(D) Immunoblot analysis for PIAS3 in lysates from IECs and tumors of WT and IRAK-M^{-/-} mice after AOM/DSS treatment (day 63). β-Actin represents the loading control.

(E) Immunoblot analysis after isolation of SUMOylated proteins for phospho-STAT3 and STAT3 in lysates from tumors of WT and IRAK-M^{-/-} mice ± proteasome inhibitor bortezomib after AOM/DSS treatment (day 63). β-Actin represents the loading control.

(F) In situ proximity ligation assay of STAT3 and IRAK-M in human CRC tissue.

(G) Immunoblot analysis for caspase-3 in lysates from IECs and tumors of WT and IRAK-M^{-/-} mice after AOM/DSS treatment (day 63). β-Actin represents the loading control.

(H) TUNEL assay of tumors of WT and IRAK-M^{-/-} mice after AOM/DSS colitis (day 63).

Scale bars, 50 μm. See also Figure S4.

growth in IRAK-M^{-/-} mice. Therefore, we analyzed pathways that are known to be critical in the pathogenesis of CRC. We have already shown above that the NF-κB pathway is similar in AOM/DSS-treated IRAK-M^{-/-} mice compared with WT mice (Figure S1G). Another pathway that is important for sustained progression of tumor growth is the STAT3 pathway. STAT3 acts as an oncogene and is a key player linking inflammation and cancer. We demonstrated that total STAT3 protein is decreased or absent in IRAK-M-deficient tumors and, consequently, activated STAT3 protein is also reduced in IRAK-M-deficient tumors (Figures 4A, 4B, and S4A). Furthermore, we characterized several downstream targets of the STAT3 pathway, which are critical regulators of cell-cycle progression, proliferation, and apoptosis (Hsp70, c-myc, Cyclin D1, Bax2, Survivin, Bcl-2, Bcl-xL) and STAT3-dependent cytokines (IL-6, IL-11) (Figures 4C, S4B, and S4C). Whereas the downstream targets of STAT3 are decreased in IRAK-M-deficient tumors (Figure 4C), the cytokines IL-6 and IL-11 show no changes in their secretion levels (Figures S4B and S4C). A known inhibitor

of STAT3 is PIAS3 (protein inhibitor of activated STAT3), which acts as an E3 SUMO ligase. Analysis of PIAS3 expression in IRAK-M^{-/-} tumors revealed a strong upregulation of PIAS3 protein expression compared with WT tumors (Figure 4D). As PIAS3 is an E3 SUMO ligase, we hypothesized that elevated PIAS3 in IRAK-M^{-/-} tumors SUMOylates STAT3 in tumor cells to induce its proteasomal degradation. To test this hypothesis, we administered the proteasome inhibitor bortezomib for the last two days of the course of AOM/DSS colitis to prevent degradation of SUMOylated proteins. From protein lysates of IRAK-M-deficient and WT tumors we isolated SUMOylated proteins and analyzed whether STAT3 is among the SUMOylated proteins in IRAK-M-deficient tumors. Indeed, we were able to show strong accumulation of SUMOylated STAT3 and SUMOylated activated STAT3 specifically in IRAK-M^{-/-} tumors, whereas WT tumors showed similar levels of SUMOylated STAT3 irrespective of bortezomib (Figure 4E). Next, we wondered whether IRAK-M can interact with STAT3 directly. To verify this hypothesis, we performed in situ proximity ligation assays on human CRC

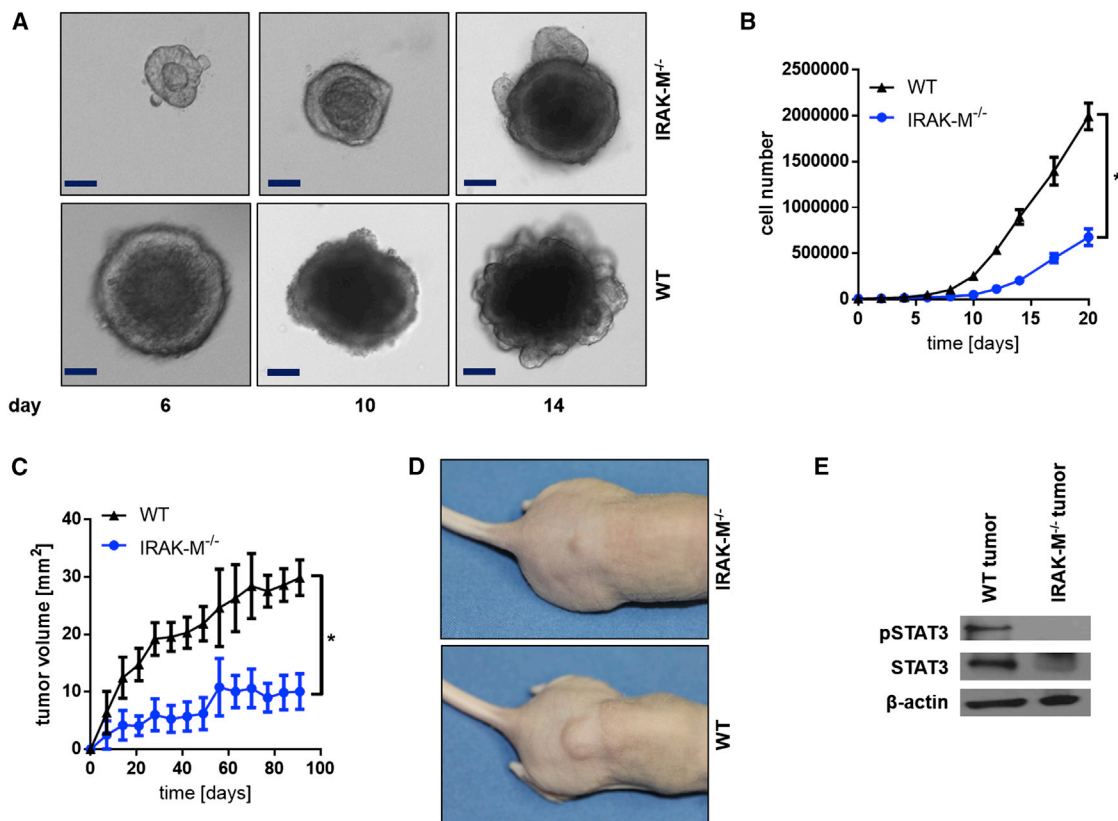


Figure 5. IRAK-M Also Fuels Tumorigenesis in an Uninflamed Tumor Microenvironment

(A) Tumor organoids of WT and IRAK-M^{-/-} mice at different time points after the beginning of cultivation. Scale bar, 100 μ m.

(B) Proliferation of WT and IRAK-M^{-/-} tumor organoids. The absolute cumulative cell numbers are shown on a linear scale on the y axis. Data are mean \pm SD (n = 8) (*p \leq 0.05).

(C) Proliferation of tumor grafts of WT and IRAK-M^{-/-} tumor organoids in CrI:NU-Foxn1^{nu} mice. The absolute tumor volumes are shown on a linear scale on the y axis. Data are mean \pm SD (n = 5) (*p \leq 0.05).

(D) Tumor grafts of WT and IRAK-M^{-/-} tumor organoids in CrI:NU-Foxn1^{nu} mice at day 100 after implantation.

(E) Immunoblot analysis for phospho-STAT3 and STAT3 in lysates from tumor grafts of WT and IRAK-M^{-/-} mice. β -Actin represents the loading control.

See also Figure S5.

tissue. We indeed verified the interaction of IRAK-M with STAT3 (Figures 4F and S4D). As we have shown that prosurvival and antiapoptotic proteins are deregulated in IRAK-M^{-/-} tumors (Figure 4C), we analyzed caspase-3 activation in IRAK-M^{-/-} tumors and detected elevated levels of cleaved caspase-3, corresponding to enhanced apoptosis in IRAK-M^{-/-} tumors (Figure 4G). This was also verified by TUNEL (terminal deoxynucleotidyl transferase dUTP nick end labeling) assays (Figure 4H). Therefore, there are two different pathways regulated by IRAK-M expressed in CRC cells, the antimicrobial response and the stability of STAT3 signaling, which both explain the scenario of accelerated tumor growth in the presence of tumor cell-intrinsic IRAK-M.

IRAK-M Supports Tumorigenesis Also in Uninflamed Tumor Microenvironments

We next investigated whether IRAK-M is able to exert its effect on tumor cell proliferation independently of the microbiome, inflammation, and the orthotopic location. Therefore, we established tumor organoids of isolated colonic tumors of WT and

IRAK-M^{-/-} mice treated with AOM/DSS and performed in vitro proliferation assays. Additionally, we set up a subcutaneous tumor graft model with these tumor organoids in nude mice. Using in vitro proliferation assays, we revealed that IRAK-M-deficient tumor organoids proliferate significantly slower than WT tumor organoids (Figures 5A and 5B). In addition, IRAK-M^{-/-} tumor organoids show diminished cell proliferation in the subcutaneous tumor graft model (Figures 5C and 5D). Consistent with the observed molecular events, western blotting demonstrated that these transplanted tumor organoids are also devoid of STAT3 and phosphorylated STAT3 (Figure 5E). In addition, similar to the AOM/DSS model, IRAK-M-deficient tumors were associated with enhanced apoptosis as shown by elevated levels of cleaved caspase-3 (Figure S5).

IRAK-M Is Expressed in Tumor Cells of Human CRC Patients and Is Associated with Reduced Cancer-Specific Survival

To understand whether IRAK-M also has influence on human CRC, we performed immunohistochemistry-based tissue

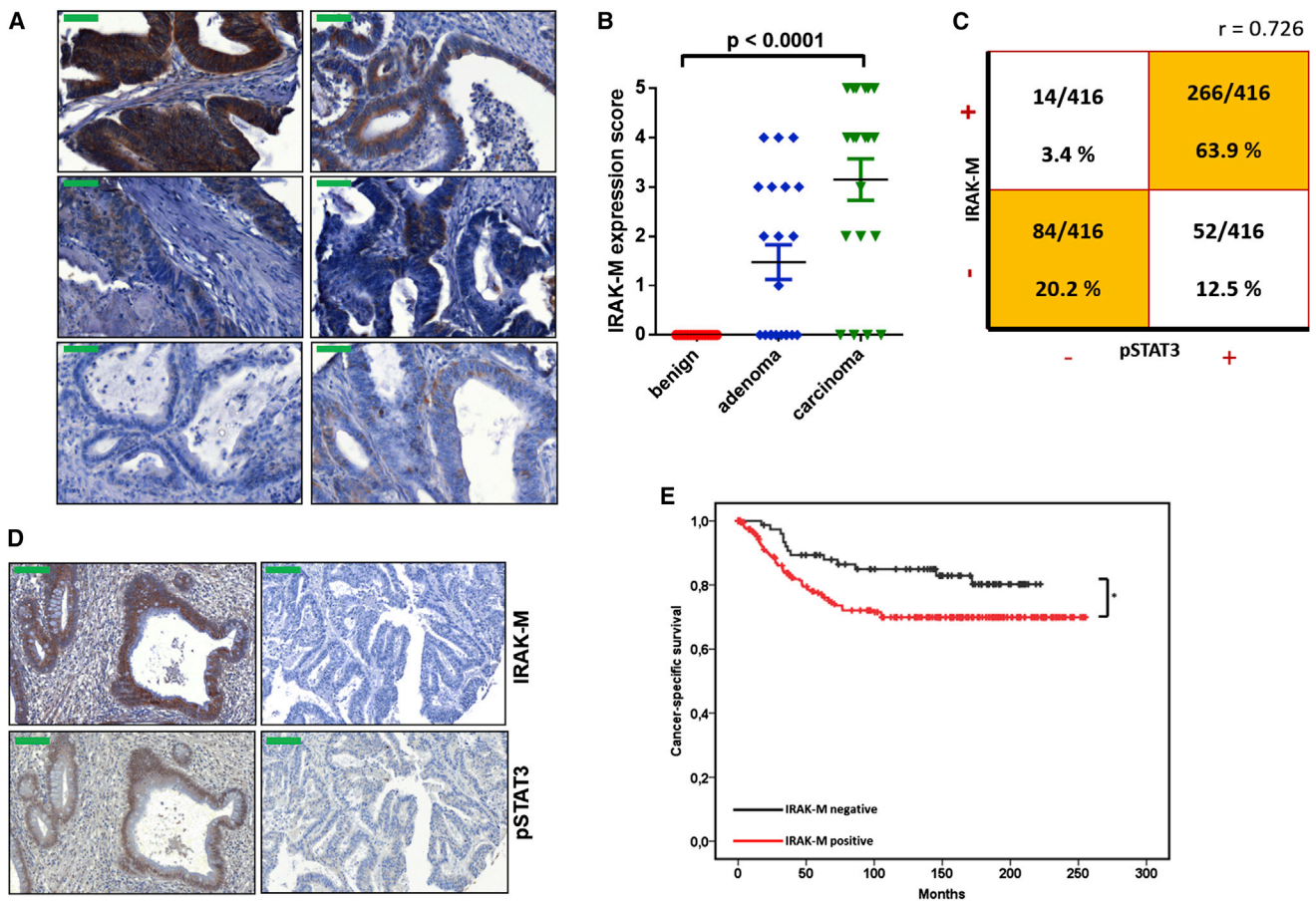


Figure 6. IRAK-M Is Expressed in Tumor Cells of Human CRC Patients and Is Associated with Reduced Cancer-Specific Survival

(A) Immunohistochemical analysis of IRAK-M expression in different samples of human CRC specimens.

(B) Analysis of IRAK-M expression in benign mucosa, adenoma, and carcinoma. Each data point represents the grade of IRAK-M expression in one patient. The horizontal bar represents the mean \pm SEM.

(C) Correlation analysis of IRAK-M and phospho-STAT3 expression in CRC patients with $r = 0.726$ and $p \leq 0.0001$.

(D) Immunohistochemical analysis of phospho-STAT3 and IRAK-M expression at the same location of one sample of a human CRC specimen.

(E) Overall survival of CRC patients with IRAK-M-positive tumor cells compared with CRC patients with IRAK-M-negative tumor cells depicted by Kaplan-Meier curve ($*p \leq 0.05$).

Scale bars, 50 μ m. See also Figure S6.

microarray analysis (TMA). We first analyzed the expression of IRAK-M in tissue sections of 323 CRC samples. We demonstrated high expression of IRAK-M in tumor cells of approximately 19% of CRC specimens, whereas others showed intermediate (57%) or no expression (24%) of IRAK-M (Figures 6A and S6A). Untransformed IECs do not express IRAK-M (Figure S6B). In inflamed colon of ulcerative colitis patients, expression of IRAK-M was limited only to immune cells (Figure S6B). To analyze the time course of IRAK-M upregulation, we analyzed different steps of CRC progression and showed that IRAK-M is already upregulated in adenomas (Figure 6B). As we have shown that IRAK-M stabilizes STAT3 protein in tumors of mice, we hypothesized that the expression of IRAK-M and STAT3 is positively correlated in human CRCs. Therefore, we analyzed IRAK-M and phosphorylated STAT3 expression in tumor cells of a second TMA containing 416 CRC patients. Correlation analysis revealed a strong positive correlation between IRAK-M and pSTAT3 in CRC, with $r = 0.762$ (Figures 6C and 6D). In addition,

we analyzed the first TMA with 323 CRC patients for IRAK-M expression and correlated the IRAK-M expression with clinical parameters (patient characteristics in Figure S6C). To this end, we first examined the relationship of IRAK-M to cancer-specific survival (Figure 6E). We revealed that CRC patients with IRAK-M-expressing tumors have a significantly worse cancer-specific survival ($p \leq 0.036$) (Figure 6E). Further evaluation of the clinical relevance of IRAK-M expression in tumor cells of CRCs revealed that there is no further association with clinical parameters such as tumor grade, tumor stage, metastasis, localization, R classification, or histological classification, suggesting that IRAK-M expression is an independent prognostic parameter for the assessment of cancer-specific survival of patients with CRC (Figure S6D). As we have shown that IRAK-M is induced through simultaneous TLR2/4 and Wnt stimulation, we analyzed whether there is a correlation between IRAK-M, active β -catenin, TLR2, and TLR4 in human CRC specimens (Figures S6E and S6F). Indeed, we found strong correlation between TLR4, IRAK-M,

and active β -catenin but a weak correlation with TLR2 (Figures S6E and S6F). In summary, we showed that the expression of IRAK-M in human CRC has similar consequences for the pathogenesis of CRC as shown earlier in murine colorectal tumors.

DISCUSSION

As early as the nineteenth century, Virchow postulated that tumors are infiltrated by immune cells (Balkwill and Mantovani, 2001). However, at the time it was not known whether tumor-infiltrating lymphocytes (TILs) are the cause of tumorigenesis or the consequence of tumor development. Today it is firmly established that inflammation fuels tumorigenesis. The inflammation-associated tumor microenvironment of CRCs is well characterized consist of different TILs as well as mesenchymal cells, various inflammatory mediators such as proinflammatory cytokines and chemokines, and genotoxic substances such as reactive oxygen and nitrogen species, all of which act in concert to fuel cancer development. Just recently another important risk factor for the development of CRC has been described, namely the gut microbiome (Arthur et al., 2012; Berglund et al., 2010; Corvinus et al., 2005). It has been shown that the microbiome affects inflammation, which in turn fuels tumorigenesis. Furthermore, the compositions of the microbiota as well as certain functional capacities of the microbes influence cancer progression (Grivennikov, 2013). However, it is not known how exactly the microbial dysbiosis affects inflammation and carcinogenesis. Intestinal mucosal immunity is continuously stimulated by the commensal microflora, and thus requires regulatory mechanisms to prevent excessive activation of innate immunity. Recently it was demonstrated that TLRs and MyD88 regulate the cancerogenesis of CRCs (Abreu, 2010; Rakoff-Nahoum and Medzhitov, 2007; Salcedo et al., 2010). Less is known about whether negative regulators of TLRs receptors affect CRC. Here we show that IRAK-M, an inhibitor of TLR signaling, is not only expressed and functional in antigen-presenting cells (APCs) but also in tumor cells of CRC, thus affecting the progression of CRCs. This tumor cell-intrinsic effect of IRAK-M is mediated by an IRAK-M-dependent increase of mucosal permeability at the tumor site and in particular by IRAK-M-dependent stabilization of STAT3 protein in colonic tumor cells.

With respect to the inflammatory response, it is already known that the absence of IRAK-M exacerbates acute colitis. In the case of acute DSS colitis, Biswas et al. (2011) described that IRAK-M deficiency led to expansion of Th1, Th17, and Treg cells. Additionally the proinflammatory cytokines IL-1 β , IL-6, and TNF were increased in IRAK-M^{-/-} mice, leading to increased susceptibility to intestinal inflammation. However, less is known about the impact of IRAK-M in chronic colitis and CRC. Here, we verify that IRAK-M is able to slightly attenuate inflammation in chronic DSS colitis; however, the major antiinflammatory effects of IRAK-M are seen in the early acute phase of colitis. In-depth analysis revealed substantial differences in the number of infiltrating leukocytes and also in the composition of immune cell subpopulations in the acute phase of inflammation, although throughout the chronic phase the extent of the differences is reduced and stable. Regarding the inflammatory response during AOM/DSS colitis, we demonstrate elevated absolute numbers of infiltrating CD45⁺ leukocytes with enhanced activa-

tion status of these cells, but almost no or only slight differences in the relative composition of the distinct immune cell subpopulations in the absence of IRAK-M. Strikingly, IRAK-M^{-/-} mice treated with AOM/DSS (despite increased chronic colitis) develop fewer tumors. This observation is contradictory to the established concept that inflammation fuels tumorigenesis. However, in the situation of inflammation-induced tumorigenesis, the inflammation of colonic lamina propria and inflammation inside the tumor tissue can differ, as shown for example by Grivennikov et al. (2012) and Schwitala et al. (2013). Therefore, in the absence of IRAK-M the increased inflammatory response is not sufficient to constitute a tumor microenvironment that can overcome major defects in tumor progression pathways in IRAK-M^{-/-} mice (i.e., massively enhanced antimicrobial response and accumulation of mucins at the tumor site and, in particular, loss of STAT3 signaling in the tumor cell) and consequently drive inflammation-associated tumorigenesis. Due to the observed dichotomy between inflammation and tumor formation, we conclude that upon loss of the intact STAT3 signaling pathway in IRAK-deficient tumor cells, reduced tumor cell proliferation, increased tumor cell apoptosis, and reduced angiogenesis lead to low tumor load of the colons. The affected tumor cell-intrinsic mechanisms are superior to the inflammatory tumor milieu in supporting tumor growth. This idea is supported by the BM chimera studies. On the one hand, we showed that the strong inflammatory responses in mice deficient for IRAK-M in the hematopoietic system indeed contributes to a progression of colonic tumors, when the irradiation-insensitive compartment (including the colonic epithelium) is IRAK-M sufficient and therefore has an intact STAT3 signaling pathway. On the other hand, when tumors are IRAK-M-deficient (IRAK-M deficiency in the irradiation-insensitive compartment) and therefore lack an intact STAT3 signaling pathway, tumor progression is suspended irrespective of the extent of the underlying inflammatory response.

IRAK-M expression was thought to be mainly confined to the monocyte and macrophage lineage. Within the population of APCs it was shown that IRAK-M is induced through TLR ligation by commensal bacteria (Biswas et al., 2011). In this study we demonstrate that IRAK-M can also be expressed in tumor cells, whereas non-tumorous colonic epithelial cells show no upregulation of IRAK-M through TLR ligation alone. IRAK-M can be induced in epithelial cells through TLR2 or TLR4 ligation when combined with Wnt activation; thus explaining the expression of IRAK-M in tumor cells of CRC, as the aberrant activation of the Wnt pathway is most commonly the initiating event of intestinal carcinogenesis leading to stabilization of β -catenin. Therefore, we suggest that IRAK-M has a critical role in providing controlled feedback to bacteria in CRCs. It is well described that TLRs promote CRC progression through epithelial cells, stromal fibroblasts, and immune cells. A key cancer-promoting effect of TLR signaling is the induction of the main survival pathways of CRC, the NF- κ B and STAT3 signaling pathways. TLR4, the receptor for lipopolysaccharide (LPS), a Gram-negative bacterial cell wall component, promotes carcinogenesis, as shown by reduced tumor development in TLR4-deficient mice and by increased tumor load in mice expressing constitutively activated epithelial TLR3 (Fukata et al., 2007). TLR2, which recognizes peptidoglycan and lipoteichoic acid, has been shown to promote gastric cancer (Tye et al., 2012). We have revealed that tumors of

IRAK-M^{-/-} mice show highly aberrant antibacterial responses. In line with this finding, IRAK-M^{-/-} mice suffering from CAC have fewer luminal bacteria, as well as reduced species richness in the bacteria infiltrating the colonic or tumor tissue compared with WT mice. Furthermore, the diversity of the IRAK-M^{-/-}-associated microbiome is also different from the WT-associated microbiome. The lack of *Roseburia*, *Blautia*, and *Eubacterium* in IRAK-M^{-/-} mice is consistent with the findings of other research groups that show a reduction of anaerobic commensal microbes in inflammatory bowel diseases and CRC (Baek et al., 2014; Irrazabal et al., 2014; Liang et al., 2014). *Roseburia* and *Eubacterium* are described to be protective and immunosuppressive, as they stimulate mucus secretion and produce short-chain fatty acids such as butyrate (Irrazabal et al., 2014; Singh et al., 2014). Also, however, *Blautia* is known to act protectively through production of acetate. Therefore, we have shown that there is a discrepancy in the IRAK-M^{-/-} mice concerning microbial profile and CRC development. The IRAK-M^{-/-} mice show a typical profile that is described to be associated with colitis and CRC but indeed shows less tumor development. However, the basis for these differences in the microbiome and its consequences for colitis and CRC pathogenesis need to be studied in future. It has already been shown in NOD2^{-/-} and Rag2/T-bet^{-/-} mice that colitis triggered by bacterial dysbiosis is transmissible (Couturier-Maillard et al., 2013; Garrett et al., 2007). The transmission of tumors through the exchange of the disturbed microbiota of NOD2^{-/-} mice has also been verified (Couturier-Maillard et al., 2013). Here, we verified that the colitis of IRAK-M-deficient mice is also transmissible to WT mice through co-housing of WT and IRAK-M^{-/-} mice. However, the tumorigenesis in IRAK-M^{-/-} mice is not altered when IRAK-M^{-/-} mice are exposed to WT microbiota. These observations revealed that IRAK-M has an important role in shaping a protective microbiota composition to safeguard against colitis. The independence of the underlying microbiota in IRAK-M-deficient mice underscores the fundamental importance of the tumor cell-intrinsic effect of IRAK-M and explains the observed dichotomy between inflammation and tumor formation in the absence of IRAK-M. A key pathway involved in the progression of colitis-associated colorectal carcinogenesis and, thereby, contributing to the link between inflammation and cancer progression, is the STAT3 pathway. Bollrath et al. (2009) showed that conditional deletion of STAT3 in IECs provides protection against CRC, whereas constitutively activated STAT3 promotes intestinal tumor growth. This could be explained by the fact that STAT3 provides pro-survival and proliferation signals for tumor cells. Recently, it has been described that activated STAT3 promotes the expression of the histone 3 lysine 79 (H3K79) methyltransferase DOT1L in CRC (Kryczek et al., 2014). DOT1L induces stem cell genes, resulting in increased cancer stemness and tumorigenic potential of CRC (Kryczek et al., 2014). In IRAK-M^{-/-} mice we demonstrated that STAT3 protein is disrupted in tumors. Due to the loss of STAT3-associated pro-survival signals, IRAK-M-deficient tumors are accompanied by exaggerated apoptosis. The disruption of STAT3 is associated with an upregulation of PIAS3, the repressor of the activity of STAT3. The major function of PIAS3 is its action as SUMO E3 ligase. Analogous to this function of PIAS3, we revealed that SUMOylated STAT3 is degraded through the proteasome in IRAK-M^{-/-} mice, whereas there is

no SUMOylation and proteasomal degradation of STAT3 in WT tumors. The disruption of STAT3 stability through loss of IRAK-M explains the observed diminished tumorigenesis in IRAK-M^{-/-} mice. STAT3 is a key regulatory molecule not merely in CAC but also in spontaneous CRC (Schwitalla et al., 2013). Schwitalla et al. (2013) showed that in spontaneous colorectal carcinogenesis an inflammatory microenvironment is generated and accompanied by a strong accumulation of phosphorylated STAT3 at the invasion front. STAT3 is thought to control proliferation, survival, and metastatic spread in this model. In line with these observations, we showed that IRAK-M^{-/-} tumors proliferate less in vitro and in vivo without preinduction of inflammation. In human CRC samples, increased activation of STAT3 has also been reported, and the activation is associated with an increased dedifferentiation and proliferation of tumor cells (Corvinus et al., 2005). Therefore, STAT3 activation correlates with poor prognosis in patients with CRC (Kusaba et al., 2006; Morikawa et al., 2011). Moreover, in colon cancer patients the degree of invasion and the occurrence of lymphatic metastases correlate with activation of STAT3 (Kusaba et al., 2005). Here, we showed that IRAK-M is also expressed in human CRC cells, and STAT3 and IRAK-M expression are positively correlated in CRC patients. Approximately 75% of CRC patients show IRAK-M positivity in their tumor cells. We hypothesized that IRAK-M expression is regulated by the microbiome; therefore, we suggest that the 25% IRAK-M-negative tumor cells have less bacterial infiltration in the tumoral regions. Overall, IRAK-M expression and consecutively correlated STAT3 expression are associated with a worse overall survival and worse cancer-specific survival in CRC patients.

In conclusion, we have demonstrated a functional role for IRAK-M in CRC, as IRAK-M is a key molecule regulating STAT3 stability in CRC and therefore influences the cancer-specific survival of patients. IRAK-M is an independent prognosticator of the survival of patients with CRC and represents an interesting target for the development of future therapeutic strategies.

EXPERIMENTAL PROCEDURES

Human Samples

Biopsy specimens were taken from routine endoscopic examinations. Tumor resected tissue was taken from tumor surgery. This study was conducted according to the principles expressed in the Declaration of Helsinki and was approved by the local ethics committee of the University of Regensburg (#14-101-0014). All patients included in this study gave written informed consent.

Mouse Breeding

B6.IRAK-M^{-/-}, CD45.1^{+/+} (B6.SJL-Ptprc^aPep3^b/BoyJ), B6.Vil-Cre, B6.p53^{fl/fl}, Crl:NU-Foxn1^{nu}, and C57BL/6 mice were purchased from Charles River and bred and maintained in the central animal facility of the University of Regensburg. Vil-Cre mice were crossed with p53^{fl/fl} mice to generate Vil-Cre × p53^{fl/fl} mice (Tp53^{ΔIEC} mice). Mice were handled according to established University of Regensburg institutional guidelines under the authority of a license of the Government of Upper Palatinate, Bavaria.

Statistics

Before statistical analysis, normal distribution was tested with the Kolmogorov-Smirnov test. Normal distributed data were evaluated with standard two-tailed Student's *t* tests with *p* values of ≤0.05 considered marginally significant. For data not showing a normal distribution, we used Wilcoxon-Mann-Whitney tests

for statistical analysis. We evaluated the statistics with SPSS Statistics software. GraphPad Prism was used to calculate the SD between experimental datasets containing equal number of replicates. Correlation studies were analyzed with Spearman's correlation.

ACCESSION NUMBERS

Microbiome data are accessible through the European Nucleotide Archive under the number ENA: PRJEB8425.

SUPPLEMENTAL INFORMATION

Supplemental Information includes Supplemental Experimental Procedures and six figures and can be found with this article online at <http://dx.doi.org/10.1016/j.ccell.2016.03.014>.

AUTHOR CONTRIBUTIONS

R.K. designed and performed the experiments. R.K. and S.F.F. analyzed data, provided overall direction, and wrote the manuscript. S.F.F. provided funding for the study. J.G., A.H., C.S., and S.B. helped with experiments. A.K.W. provided support with the BM chimera study. E.N., S.M., R.S.C., and M.S. provided tissue microarray of human samples and analyzed the clinical data. J.G., A.H., and A.G. performed and analyzed the microbiome studies. H.N. and M.F.N. provided human biopsy samples. C.H. provided support with the human CRC cell lines. G.K. provided support with the tumor graft model. H.J.S. and E.K.K. discussed findings.

ACKNOWLEDGMENTS

We would like to thank all members of the Laboratory of Chronic Immunopathology for critical discussions, especially Manuela Kovács-Sauter, Marcus Kielmanowicz, Marlene Rosendahl, and Tatjana Schifferstein for skillful technical assistance and general support. This project was supported by grant Fi1526/4-1 and Fi1526/5-1 from the Deutsche Forschungsgemeinschaft and by the Regensburg Center of Interventional Immunology. Further, this work was supported by a grant from the Deutsche Forschungsgemeinschaft (KFO 257 CEDER STU238/6-1) to M.S. and the German Cancer Aid (109510) to M.S. and E.N. The authors gratefully acknowledge this support.

Received: February 23, 2015

Revised: August 12, 2015

Accepted: March 18, 2016

Published: April 14, 2016

REFERENCES

- Abreu, M.T. (2010). Toll-like receptor signalling in the intestinal epithelium: how bacterial recognition shapes intestinal function. *Nat. Rev. Immunol.* *10*, 131–144.
- Arthur, J.C., and Jobin, C. (2013). The complex interplay between inflammation, the microbiota and colorectal cancer. *Gut Microbes* *4*, 253–258.
- Arthur, J.C., Perez-Chanona, E., Muhlbauer, M., Tomkovich, S., Uronis, J.M., Fan, T.J., Campbell, B.J., Abujamal, T., Dogan, B., Rogers, A.B., et al. (2012). Intestinal inflammation targets cancer-inducing activity of the microbiota. *Science* *338*, 120–123.
- Baek, S.J., Kim, S.H., Lee, C.K., Roh, K.H., Keum, B., Kim, C.H., and Kim, J. (2014). Relationship between the severity of diversion colitis and the composition of colonic bacteria: a prospective study. *Gut Liver* *8*, 170–176.
- Balkwill, F., and Mantovani, A. (2001). Inflammation and cancer: back to Virchow? *Lancet* *357*, 539–545.
- Ben-Neriah, Y., and Karin, M. (2011). Inflammation meets cancer, with NF-kappaB as the matchmaker. *Nat. Immunol.* *12*, 715–723.
- Berglund, M., Melgar, S., Kobayashi, K.S., Flavell, R.A., Hornquist, E.H., and Hultgren, O.H. (2010). IL-1 receptor-associated kinase M downregulates DSS-induced colitis. *Inflamm. Bowel Dis.* *16*, 1778–1786.
- Biswas, A., Wilmanski, J., Forsman, H., Hrcir, T., Hao, L., Tlaskalova-Hogenova, H., and Kobayashi, K.S. (2011). Negative regulation of Toll-like receptor signaling plays an essential role in homeostasis of the intestine. *Eur. J. Immunol.* *41*, 182–194.
- Bollrath, J., and Greten, F.R. (2009). IKK/NF-kappaB and STAT3 pathways: central signalling hubs in inflammation-mediated tumour promotion and metastasis. *EMBO Rep.* *10*, 1314–1319.
- Bollrath, J., Pheesse, T.J., von Burstin, V.A., Putoczki, T., Bennecke, M., Bateman, T., Nebelsiek, T., Lundgren-May, T., Canli, O., et al. (2009). gp130-mediated Stat3 activation in enterocytes regulates cell survival and cell-cycle progression during colitis-associated tumorigenesis. *Cancer Cell* *15*, 91–102.
- Clevers, H. (2004). At the crossroads of inflammation and cancer. *Cell* *118*, 671–674.
- Corvinus, F.M., Orth, C., Moriggi, R., Tsareva, S.A., Wagner, S., Pfitzner, E.B., Baus, D., Kaufmann, R., Huber, L.A., Zatloukal, K., et al. (2005). Persistent STAT3 activation in colon cancer is associated with enhanced cell proliferation and tumor growth. *Neoplasia* *7*, 545–555.
- Couturier-Maillard, A., Secher, T., Rehman, A., Normand, S., De Arcangelis, A., Haesler, R., Huot, L., Grandjean, T., Bressenot, A., Delanoye-Crespin, A., et al. (2013). NOD2-mediated dysbiosis predisposes mice to transmissible colitis and colorectal cancer. *J. Clin. Invest.* *123*, 700–711.
- Fukata, M., and Abreu, M.T. (2009). Pathogen recognition receptors, cancer and inflammation in the gut. *Curr. Opin. Pharmacol.* *9*, 680–687.
- Fukata, M., and Arditi, M. (2013). The role of pattern recognition receptors in intestinal inflammation. *Mucosal Immunol.* *6*, 451–463.
- Fukata, M., Chen, A., Vamadevan, A.S., Cohen, J., Breglio, K., Krishnareddy, S., Hsu, D., Xu, R., Harpaz, N., Dannenberg, A.J., et al. (2007). Toll-like receptor-4 promotes the development of colitis-associated colorectal tumors. *Gastroenterology* *133*, 1869–1881.
- Fukata, M., Shang, L., Santaolalla, R., Sotolongo, J., Pastorini, C., Espana, C., Ungaro, R., Harpaz, N., Cooper, H.S., Elson, G., et al. (2011). Constitutive activation of epithelial TLR4 augments inflammatory responses to mucosal injury and drives colitis-associated tumorigenesis. *Inflamm. Bowel Dis.* *17*, 1464–1473.
- Gallimore, A.M., and Godkin, A. (2013). Epithelial barriers, microbiota, and colorectal cancer. *N. Engl. J. Med.* *368*, 282–284.
- Garrett, W.S., Lord, G.M., Punit, S., Lugo-Villarino, G., Mazmanian, S.K., Ito, S., Glickman, J.N., and Glimcher, L.H. (2007). Communicable ulcerative colitis induced by T-bet deficiency in the innate immune system. *Cell* *131*, 33–45.
- Goel, G.A., Kandiel, A., Achkar, J.P., and Lashner, B. (2011). Molecular pathways underlying IBD-associated colorectal neoplasia: therapeutic implications. *Am. J. Gastroenterol.* *106*, 719–730.
- Grivnenkov, S.I. (2013). Inflammation and colorectal cancer: colitis-associated neoplasia. *Semin. Immunopathol.* *35*, 229–244.
- Grivnenkov, S.I., Wang, K., Mucida, D., Stewart, C.A., Schnabl, B., Jauch, D., Taniguchi, K., Yu, G.Y., Osterreicher, C.H., Hung, K.E., et al. (2012). Adenoma-linked barrier defects and microbial products drive IL-23/IL-17-mediated tumour growth. *Nature* *491*, 254–258.
- Irrazabal, T., Belcheva, A., Girardin, S.E., Martin, A., and Philpott, D.J. (2014). The multifaceted role of the intestinal microbiota in colon cancer. *Mol. Cell* *54*, 309–320.
- Jobin, C. (2013). Colorectal cancer: looking for answers in the microbiota. *Cancer Discov.* *3*, 384–387.
- Kobayashi, K., Hernandez, L.D., Galan, J.E., Janeway, C.A., Jr., Medzhitov, R., and Flavell, R.A. (2002). IRAK-M is a negative regulator of Toll-like receptor signaling. *Cell* *110*, 191–202.
- Kryczek, I., Lin, Y., Nagarsheth, N., Peng, D., Zhao, L., Zhao, E., Vatan, L., Szeliga, W., Dou, Y., Owens, S., et al. (2014). IL-22(+)/CD4(+) T cells promote colorectal cancer stemness via STAT3 transcription factor activation and induction of the methyltransferase DOT1L. *Immunity* *40*, 772–784.
- Kusaba, T., Nakayama, T., Yamazumi, K., Yakata, Y., Yoshizaki, A., Nagayasu, T., and Sekine, I. (2005). Expression of p-STAT3 in human colorectal

- adenocarcinoma and adenoma; correlation with clinicopathological factors. *J. Clin. Pathol.* **58**, 833–838.
- Kusaba, T., Nakayama, T., Yamazumi, K., Yakata, Y., Yoshizaki, A., Inoue, K., Nagayasu, T., and Sekine, I. (2006). Activation of STAT3 is a marker of poor prognosis in human colorectal cancer. *Oncol. Rep.* **15**, 1445–1451.
- Liang, X., Li, H., Tian, G., and Li, S. (2014). Dynamic microbe and molecule networks in a mouse model of colitis-associated colorectal cancer. *Sci. Rep.* **4**, 4985.
- McDermott, A.J., and Huffnagle, G.B. (2014). The microbiome and regulation of mucosal immunity. *Immunology* **142**, 24–31.
- Morikawa, T., Baba, Y., Yamauchi, M., Kuchiba, A., Nosho, K., Shima, K., Tanaka, N., Huttenhower, C., Frank, D.A., Fuchs, C.S., and Ogino, S. (2011). STAT3 expression, molecular features, inflammation patterns, and prognosis in a database of 724 colorectal cancers. *Clin. Cancer Res.* **17**, 1452–1462.
- Ohtani, N. (2014). Microbiome and cancer. *Semin. Immunopathol.* **37**, 65–72.
- Pandey, S., Kawai, T., and Akira, S. (2014). Microbial sensing by toll-like receptors and intracellular nucleic acid sensors. *Cold Spring Harbor Perspect. Biol.* **7**, a016246.
- Rakoff-Nahoum, S., and Medzhitov, R. (2007). Regulation of spontaneous intestinal tumorigenesis through the adaptor protein MyD88. *Science* **317**, 124–127.
- Salcedo, R., Worschech, A., Cardone, M., Jones, Y., Gyulai, Z., Dai, R.M., Wang, E., Ma, W., Haines, D., O’Hugin, C., et al. (2010). MyD88-mediated signaling prevents development of adenocarcinomas of the colon: role of interleukin 18. *J. Exp. Med.* **207**, 1625–1636.
- Schwitalla, S., Ziegler, P.K., Horst, D., Becker, V., Kerle, I., Begus-Nahrman, Y., Lechel, A., Rudolph, K.L., Langer, R., Slotta-Huspenina, J., et al. (2013). Loss of p53 in enterocytes generates an inflammatory microenvironment enabling invasion and lymph node metastasis of carcinogen-induced colorectal tumors. *Cancer Cell* **23**, 93–106.
- Shao, L., Oshima, S., Duong, B., Advincula, R., Barrera, J., Malynn, B.A., and Ma, A. (2013). A20 restricts wnt signaling in intestinal epithelial cells and suppresses colon carcinogenesis. *PLoS One* **8**, e62223.
- Shibolet, O., and Podolsky, D.K. (2007). TLRs in the Gut. IV. Negative regulation of Toll-like receptors and intestinal homeostasis: addition by subtraction. *Am. J. Physiol. Gastrointest. Liver Physiol.* **292**, G1469–G1473.
- Singh, N., Gurav, A., Sivaprakasam, S., Brady, E., Padia, R., Shi, H., Thangaraju, M., Prasad, P.D., Manicassamy, S., Munn, D.H., et al. (2014). Activation of Gpr109a, receptor for niacin and the commensal metabolite butyrate, suppresses colonic inflammation and carcinogenesis. *Immunity* **40**, 128–139.
- Tye, H., Kennedy, C.L., Najdovska, M., McLeod, L., McCormack, W., Hughes, N., Dev, A., Sievert, W., Ooi, C.H., Ishikawa, T.O., et al. (2012). STAT3-driven upregulation of TLR2 promotes gastric tumorigenesis independent of tumor inflammation. *Cancer Cell* **22**, 466–478.
- Xiao, H., Gulen, M.F., Qin, J., Yao, J., Bulek, K., Kish, D., Altuntas, C.Z., Wald, D., Ma, C., Zhou, H., et al. (2007). The Toll-interleukin-1 receptor member SIGIRR regulates colonic epithelial homeostasis, inflammation, and tumorigenesis. *Immunity* **26**, 461–475.